

Geometric–Optical Throughput and Étendue Revisited: Introducing the Optogeometric Factor for Pixel–Level Quantitative Imaging

Jan Sova¹ and Marie Kolaříková¹

¹Czech Technical University in Prague, Faculty of Mechanical Engineering

August 14, 2025

Abstract

This paper formally defines *optogeometric factor* F_{opg} as a pixel–level measure of geometric–optical throughput with units of $\text{m}^2 \text{sr}$.

The quantity is formally defined as the surface solid angle integral of the local étendue between a pixel and its corresponding scene element. Under ideal geometric optical conditions, it can be approximated by the product of the projected pixel footprint area on the object plane and the solid angle covered by the entrance pupil. Provides a compact link between the radiance of the scene and the radiant flux collected by a single pixel, making explicit the spatial–angular coupling that governs the radiometric measurements at the pixel level.

Two mathematically equivalent expressions of F_{opg} are derived: a *scene–based* form, expressed via the footprint area and instantaneous field of view, and a *sensor–based* form, expressed via the pixel pitch and optical f-number. Their equivalence is demonstrated analytically and confirmed using representative parameters of real thermal imaging systems.

The concept is extended to *effective optogeometric factor* $F_{\text{opg,eff}}$, which incorporates the pixel fill factor to account for the active area of the sensor. This concept enables a clear separation of geometric–optical coupling from detector design and other calibration terms, offering a physically transparent and transferable basis for quantitative thermography and other imaging modalities operating in the geometric–optics regime.

Keywords: optogeometric factor, pixel-level radiometry, quantitative thermography, radiometric calibration, geometric–optical coupling, fill factor

Contents

1	Introduction	2
2	Motivation and formulation from previous work	3
3	Optogeometric factor: geometric–optical coupling per pixel	5
3.1	Scene–Sensor Equivalence of the Optogeometric Factor	6
3.2	Derivation of the general pixel footprint on the Object Plane	8
3.3	Geometrical (scene-based) derivation of the optogeometric factor	10
3.4	Optical (sensor-based) derivation	11
3.5	Summary, comparison and special case	13
3.6	Example determination of the optogeometric factor for real thermal imaging systems	14
3.7	Effective optogeometric factor	15
4	Discussion	16
4.1	Occurrence of the Optogeometric Factor in Literature	16
4.2	Paradigm Shift in Quantitative Thermography and Radiometry	17
4.3	Limitations and Conditions of Validity	18
4.4	Analogy to Electrical Resistance	19
4.5	Illustrative example (approximate): uniform blackbody scene	19
5	Conclusion	20

1 Introduction

In quantitative imaging, such as infrared thermography, accurately relating the radiant flux received by a detector pixel to the radiance of the observed surface requires explicit specification of a geometric–optical throughput term. This term accounts for (i) the solid angle over which the pixel collects radiation from the scene and (ii) the effective projection of the corresponding scene area onto the object or image plane. Together, these factors define the spatial–angular coupling that governs signal formation in the optical path of an imaging system.

We refer to this combined quantity as the *optogeometric factor* $F_{\text{opg}}^{(\text{scene})}$ [$\text{m}^2 \text{sr}$], formally defined in the *scene-based formulation* as the surface–solid–angle integral

$$F_{\text{opg}}^{(\text{scene})} := \iint_{A_{\text{fp}}} \iint_{\Omega_{\text{pix}}(\mathbf{r})} \cos \theta \, d\Omega \, dA, \quad (1)$$

where A_{fp} is the projected pixel footprint area in the object plane, and $\Omega_{\text{pix}}(\mathbf{r})$ is the local solid angle that the entrance pupil appears to cover when seen from the point \mathbf{r} on the footprint.

This relationship was implicitly introduced in [1] in the field of thermography during the derivation of the quantitative thermography equation. Its original purpose was to enable quantitative correction for non-normal measurements, for example when measuring

temperature during resistance spot welding [2] or when imaging using UAVs [7]. However, it soon became evident that both the quantitative thermography equation and the optogeometric factor have significantly broader applicability.

Under ideal geometric–optical conditions (planar scene, uniform radiance, paraxial approximation), Eq. (1) reduces to

$$F_{\text{opg}}^{(\text{scene})} \approx A_{\text{fp}} \cdot \Omega_{\text{pix}}, \quad (2)$$

with Ω_{pix} computed from the instantaneous field of view (iFOV) as the solid angle covered by a single pixel, which in the paraxial approximation reduces to $\Omega_{\text{pix}} \approx (\varphi_{\text{iFOV}})^2$ for square pixels [4, 10].

In previous work [1], $F_{\text{opg}}^{(\text{scene})}$ appeared only implicitly within a generalized quantitative thermography equation. The present study makes the quantity explicit by providing its formal scene–based definition and deriving its approximate form $\tilde{F}_{\text{opg}}^{(\text{scene})}$ in terms of the pixel footprint and collection solid angle.¹ In addition to the scene–based formulation, an equivalent sensor–based expression $F_{\text{opg}}^{(\text{sensor})}$ is derived. The geometric and optical conditions under which $F_{\text{opg}}^{(\text{scene})} = F_{\text{opg}}^{(\text{sensor})}$ are identified, along with their respective approximate forms expressed through practical system parameters such as the pixel–pitch–to–f–number ratio or the product of entrance pupil diameter and iFOV.

Finally, the formulation is extended by defining the *effective optogeometric factor*, which incorporates the pixel fill factor to account for the finite photosensitive area of real detector pixels.

2 Motivation and formulation from previous work

In a recent publication [1], the optogeometric factor was denoted A_x in a reduced form as $1/\pi$, primarily to facilitate comparison with the conceptual thermography equation. In the present work, the more descriptive notation F_{opg} [m^2sr] is adopted, using the non-reduced form with the explicit π ,

$$F_{\text{opg}} \equiv \frac{\pi}{4} \left(D \varphi_{\text{iFOV}} \right)^2, \quad (3)$$

which directly reflects the physical meaning of the quantity, where D [m] is the entrance pupil diameter (Fig. 2), and φ_{iFOV} [rad]² is the instantaneous field of view of a single pixel [5, 6, 20]. The pixel pitch a_{pix} [m] is the centre-to-centre spacing between pixels, including any non-sensitive borders, and typically exceeds the active area size (Fig. 3).

Under the pinhole camera model and the small-angle approximation (validity discussed in 4.3),

¹The tilde notation \tilde{F}_{opg} denotes an approximate value valid only under a defined set of geometric and optical assumptions, whereas F_{opg} denotes the exact value.

² φ_{iFOV} is the instantaneous field of view per pixel in radians (Fig. 1). Squared, it approximates the solid angle subtended by the pixel, $\Omega_{\text{pix}} \approx \varphi_{\text{iFOV}}^2$, introducing steradian units into the geometric formulation of F_{opg} .

$$\varphi_{\text{iFOV}} \approx \frac{a_{\text{pix}}}{f}, \quad (4)$$

where f [m] is the focal length. The angular pixel size is assumed identical in both horizontal and vertical directions, i.e. $\varphi_{\text{iFOV}} = \varphi_{\text{iFOV,h}} = \varphi_{\text{iFOV,v}}$. The measurement scheme in Fig. 1 illustrates a pixel observing a planar target at an inclination angle α [°] in the x -axis direction.

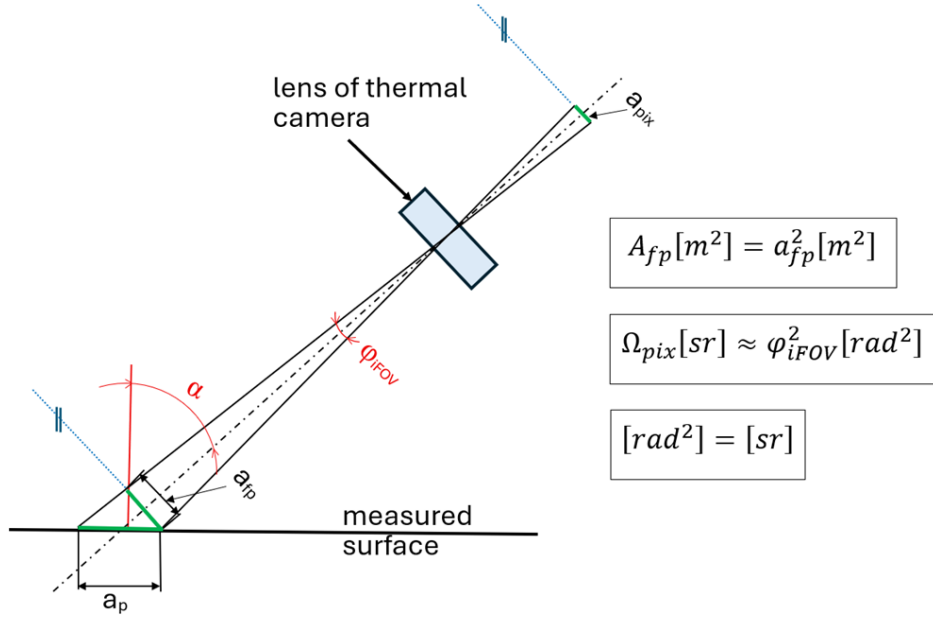


Figure 1: Measurement geometry for defining φ_{iFOV} [rad] and the projected footprint a_{fp}^2 [m²]. A pixel with pitch a_{pix} [m] observes the object surface at inclination α [°] through optics of focal length f [m]. In this single-axis tilt geometry, the inclination angle α coincides with the zenith angle θ used in radiometric calculations. Under the pinhole model, $\varphi_{\text{iFOV}} = a_{\text{pix}}/f$ [10].

The entrance pupil diameter is related to the focal length via the f-number $f\#$ [-] [10, 14]:

$$D \equiv \frac{f}{f\#}. \quad (5)$$

Substituting Eqs. (4) and (5) into Eq. (3) yields

$$F_{\text{opg}} \equiv \frac{\pi}{4} \left(\frac{f}{f\#} \right)^2 \left(\frac{a_{\text{pix}}}{f} \right)^2 = \frac{\pi}{4} \left(\frac{a_{\text{pix}}}{f\#} \right)^2. \quad (6)$$

Thus, F_{opg} can be expressed equivalently as, with the precise derivation and discussion of equivalence deferred to the subsequent analysis of the optogeometric factor:

$$F_{\text{opg}} = \frac{\pi}{4} \left(\frac{a_{\text{pix}}}{f\#} \right)^2 = \frac{\pi}{4} (D \cdot \varphi_{\text{iFOV}})^2. \quad (7)$$

In most cooled and uncooled thermal imagers, $f\#$ is fixed by optical design:

$$f\# = \frac{f}{D}, \quad (8)$$

and is optimised for high throughput (low $f\#$) while maintaining acceptable aberration control and depth of field. Consequently, $f\#$ is rarely adjustable in practice, and F_{opg} is primarily determined by a_{pix} and D . Variable apertures are found only in specialised laboratory or research instruments.

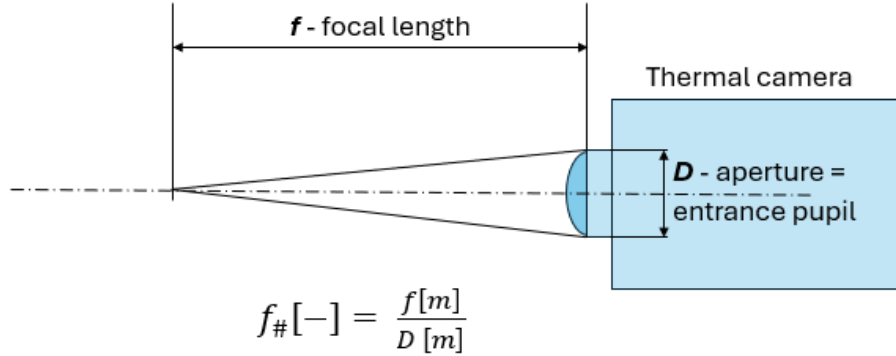


Figure 2: Entrance pupil diameter D [m] is the apparent diameter of the aperture stop as seen from object space. In fixed-aperture thermal optics, it equals the maximum usable aperture for a given focal length f [m], and is related to the f-number by $D = f/f\#$.

These two forms of F_{opg} reflect complementary viewpoints:

- **Scene-based form** (defined in Eq. (16), final form in Eq. (32)) — natural from the *scene perspective*, with D and φ_{iFOV} determining the footprint and the solid angle of acceptance.
- **Sensor-based form** (defined in Eq. (17), final form in Eq. (39)) — natural from the *sensor perspective*, with a_{pix} and $f\#$ defining the optical coupling.

3 Optogeometric factor: geometric–optical coupling per pixel

In this section, F_{opg} is derived from purely geometrical considerations, providing an alternative yet fully consistent formulation and derivation to the aperture–based approach presented in [1]. The sensor–based and scene–based perspectives are shown to be two complementary views of the same underlying relationship. The conditions for their exact equivalence are examined.

- The *scene-based* form is valid when the projected pixel footprint A_{fp} on the object plane and the acceptance solid angle Ω_{pix} are known or can be modelled, and when the scene geometry satisfies the assumptions of ideal projection (planar surface, paraxial incidence, spatially uniform radiance over the footprint). This approach does not require knowledge of the sensor’s f-number or pixel pitch.

- The *sensor-based* form is valid when the pixel pitch a_{pix} and the f-number $f\#$ (or equivalently the entrance pupil diameter D and focal length f) are known from the optical design, and when the optical system operates under paraxial conditions without vignetting or aperture clipping. This approach does not require explicit knowledge of the scene geometry or radiance distribution.

In contrast to the preceding section 2, a more precise notation will be introduced here to clearly distinguish between the scene-based optogeometric factor $F_{\text{opg}}^{(\text{scene})}$ and the sensor-based form $F_{\text{opg}}^{(\text{sensor})}$, as well as between their approximate values $\tilde{F}_{\text{opg}}^{(\text{scene})}$ and $\tilde{F}_{\text{opg}}^{(\text{sensor})}$ (i.e., the notations with a tilde, for improved readability) and the exact values $F_{\text{opg}}^{(\text{scene})}$ and $F_{\text{opg}}^{(\text{sensor})}$. This distinction is not merely a matter of notation, since the equalities $\tilde{F}_{\text{opg}}^{(\text{scene})} = \tilde{F}_{\text{opg}}^{(\text{sensor})}$ and even $F_{\text{opg}}^{(\text{scene})} = F_{\text{opg}}^{(\text{sensor})}$ do not hold universally, but only under specific geometric and optical conditions that will be discussed later in this section.

3.1 Scene–Sensor Equivalence of the Optogeometric Factor

The radiometric relationship between the radiant flux Φ_{pix} [W] collected by a single detector pixel and the radiance L [$\text{W m}^{-2} \text{sr}^{-1}$] of the observed scene can be expressed in its most general form as

$$\begin{aligned} \Phi_{\text{pix}} &= \underbrace{\iint_{A_{\text{fp}}} \iint_{\Omega_{\text{pix}}(\mathbf{r})} L_{\text{scene}}(\theta, \psi; \mathbf{r}) \cos \theta \, d\Omega \, dA}_{\text{scene-based formulation}} \\ &= \underbrace{\iint_{A_{\text{pix}}} \iint_{\Omega_{\text{ap}}(\mathbf{r}')} \tau(\mathbf{r}', \theta') L_{\text{sensor}}(\theta', \psi'; \mathbf{r}') \cos \theta' \, d\Omega' \, dA'}_{\text{sensor-based formulation}}. \end{aligned} \quad (9)$$

For the *scene-based* formulation:

- A_{fp} [m^2] is the projected pixel footprint area on the object plane,
- $\Omega_{\text{pix}}(\mathbf{r})$ [sr] is the acceptance solid angle of the entrance pupil as seen from point \mathbf{r} on the footprint,
- $L_{\text{scene}}(\theta, \psi; \mathbf{r})$ [$\text{W m}^{-2} \text{sr}^{-1}$] is the directional radiance emitted by the observed scene at (θ, ψ) ,
- θ [rad] is the zenith (inclination) angle from the surface normal; ψ [rad] is the azimuth angle,
- $\cos \theta$ [–] is the Lambertian cosine factor [8, 11],
- $d\Omega$ [sr], dA [m^2] are the differential elements of solid angle and area,
- \mathbf{r} [m] is the position vector within A_{fp} .

For the *sensor-based* formulation:

- A_{pix} [m²] is the geometric area of a single pixel,
- $\Omega_{\text{ap}}(\mathbf{r}')$ [sr] is the solid angle subtended by the entrance pupil in image space,
- $\tau(\mathbf{r}', \theta')$ is the spectral-band optical transmittance for a ray arriving at (\mathbf{r}', θ') ,
- $L_{\text{sensor}}(\theta', \psi'; \mathbf{r}')$ [W m⁻² sr⁻¹] is the radiance at the sensor entrance pupil after atmospheric transmission and optical modulation, incident on \mathbf{r}' from (θ', ψ') ,
- θ' [rad], ψ' [rad] are the polar and azimuthal angles in image space,
- $\cos \theta'$ [–] is the corresponding cosine factor,
- $d\Omega'$ [sr], dA' [m²] are the differential elements in image space,
- \mathbf{r}' [m] is the position vector within A_{pix} .

The equality in (9) holds for a passive, lossless system that conserves étendue, with negligible self-emission and without clipping or vignetting. Then we can also write

If the scene radiance L_{scene} is spatially and angularly uniform over the footprint and the pixel's acceptance cone, and the optical system satisfies ideal geometric projection [15, 17], then

$$\Phi_{\text{pix}} = L_{\text{scene}} \cdot \iint_{A_{\text{fp}}} \iint_{\Omega_{\text{pix}}(\mathbf{r})} \cos \theta \, d\Omega \, dA = L_{\text{scene}} \cdot F_{\text{opg}}^{(\text{scene})}. \quad (10)$$

where

$$F_{\text{opg}}^{(\text{scene})} := \iint_{A_{\text{fp}}} \iint_{\Omega_{\text{pix}}(\mathbf{r})} \cos \theta \, d\Omega \, dA. \quad (11)$$

Analogously, from the sensor-side optics one may define

$$\Phi_{\text{pix}} = L_{\text{sensor}} \cdot \iint_{A_{\text{pix}}} \iint_{\Omega_{\text{ap}}(\mathbf{r}')} \cos \theta' \, d\Omega' \, dA' = L_{\text{sensor}} \cdot F_{\text{opg}}^{(\text{sensor})}. \quad (12)$$

where

$$F_{\text{opg}}^{(\text{sensor})} := \iint_{A_{\text{pix}}} \iint_{\Omega_{\text{ap}}(\mathbf{r}')} \cos \theta' \, d\Omega' \, dA'. \quad (13)$$

We can further state that, under the assumption of uniform radiance and constant $\cos \theta$ over the pixel footprint and its acceptance cone,

$$\iint_{A_{\text{fp}}} \iint_{\Omega_{\text{pix}}(\mathbf{r})} \cos \theta \, d\Omega \, dA \approx A_{\text{fp}} \Omega_{\text{pix}}. \quad (14)$$

Analogously, for the sensor-based formulation under paraxial conditions and a fully illuminated circular aperture

$$\iint_{A_{\text{pix}}} \iint_{\Omega_{\text{ap}}(\mathbf{r}')} \cos \theta' \, d\Omega' \, dA' \approx A_{\text{pix}} \Omega_{\text{ap}}. \quad (15)$$

Under ideal projection geometry and constant $\cos \theta$, the integrals in (11) separate, yielding

$$F_{\text{opg}}^{(\text{scene})} \approx A_{\text{fp}} \Omega_{\text{pix}} \equiv \tilde{F}_{\text{opg}}^{(\text{scene})}. \quad (16)$$

Here A_{fp} is the footprint projected into a plane parallel to the sensor (foreshortening included), and Ω_{pix} is treated as constant across A_{fp} .

Analogously, from the sensor's perspective:

$$F_{\text{opg}}^{(\text{sensor})} \approx A_{\text{pix}} \Omega_{\text{ap}} \equiv \tilde{F}_{\text{opg}}^{(\text{sensor})}, \quad (17)$$

where A_{pix} is the (active) pixel area Ω_{ap} is the acceptance solid angle set by the entrance pupil, τ is taken as constant, and $\cos \theta' \approx 1$ in the paraxial limit.

Under the validity of equality (9), the relationships (11) and (13) are also equal, i.e.,

$$F_{\text{opg}}^{(\text{scene})} = F_{\text{opg}}^{(\text{sensor})}. \quad (18)$$

3.2 Derivation of the general pixel footprint on the Object Plane

For the case of inclination only about a single axis by an angle α (so that $\alpha \equiv \theta$ in the radiometric notation), the projected footprint area entering Eq. (9) (and Eq. (14)) is

$$A_{\text{fp}}(\alpha) = \frac{A_0}{\cos \alpha} = \frac{1}{\cos \alpha} \left(\frac{a_{\text{pix}} d}{f} \right)^2 \approx \frac{(d \varphi_{\text{iFOV}})^2}{\cos \alpha}, \quad (19)$$

where $A_0 \equiv A_{\text{fp}}(0) = \left(\frac{a_{\text{pix}} d}{f} \right)^2$ [m²] is the normal-incidence footprint, a_{pix} [m] is the pixel pitch, f [m] the focal length, d [m] the object distance, and $\varphi_{\text{iFOV}} = a_{\text{pix}}/f$ [rad].

When a pixel is viewed under oblique incidence, its projected footprint on the object plane becomes geometrically enlarged compared to normal incidence. This enlargement arises purely from the projection geometry of the inclined viewing direction and is independent of any radiometric effects. It is directly relevant for direct-detection configurations or for object-plane representations in imaging systems, assuming no optical projection system is present to compensate for the angular dependence.

For a square pixel of side length a [m], the projected footprint area $A_{\text{fp}}(\theta, \varphi)$ [m²] as a function of the zenith angle θ [rad] and azimuth angle φ [rad] is given by:

Pixel footprint area for oblique viewing

$$A_{\text{fp}}(\theta, \varphi) = \frac{a^2}{\cos \theta \cos \varphi} = a^2 \cdot E(\theta, \varphi), \quad (20)$$

where $E(\theta, \varphi) \equiv \frac{1}{\cos \theta \cos \varphi}$ is the *enlargement factor*.

In the present derivation, $A_{\text{fp}}(\theta, \varphi)$ denotes the *purely geometrical* projection of the pixel onto the object plane under the ideal pinhole model. Optical effects such as distortion, vignetting, or aperture limitations are not included here; these will be incorporated later in the radiometric formulation.

The denominator in Eq. (20) accounts for the effective projection of the square pixel area as seen by an incoming particle trajectory. The $\cos(\theta)$ term captures the reduction of the effective vertical dimension of the pixel when the trajectory is inclined relative to the sensor normal, while the $\cos(\varphi)$ term accounts for the reduction along the horizontal axis due to the azimuthal tilt. The enlargement factor is thus:

$$E(\theta, \varphi) \equiv \frac{1}{\cos \theta \cos \varphi}, \quad (21)$$

and becomes unity for normal incidence ($\theta = \varphi = 0$).

The term *footprint*, as used in this work, is defined as the purely geometrical projection of a pixel in the sensor plane as seen by an incoming particle, without any optical projection. As the incidence angles increase, this footprint grows rapidly, especially as θ or φ approach 90° . Enlargement increases the probability of pixel pile-up (multiple particles contributing to the same pixel) and degrades the effective spatial resolution.

$$A_{\text{fp}}(\theta, \varphi) \equiv a^2 E(\theta, \varphi), \quad (22)$$

where a ; [m] is the pixel pitch and $E(\theta, \varphi)$; [-] is the *enlargement factor* capturing the geometrical increase of the footprint as a function of the viewing angles.

We now define the dimensionless pixel coordinates $\boldsymbol{\xi} = (\xi, \eta) \in [-\frac{1}{2}, \frac{1}{2}]^2$. The surface element on the object plane can then be written as

$$dA = a^2 E(\theta(\boldsymbol{\xi}), \varphi(\boldsymbol{\xi})) d\xi d\eta. \quad (23)$$

The formal (scene-based) definition of the optogeometric factor then reads

$$F_{\text{opg}}^{(\text{scene})} = \iint_{A_{\text{fp}}} \iint_{\Omega_{\text{pix}}(\mathbf{r})} \cos \theta d\Omega dA, \quad (24)$$

which, upon substituting the parameterization (23), becomes

$$F_{\text{opg}}^{(\text{scene})} = \int_{-1/2}^{1/2} \int_{-1/2}^{1/2} \left[\iint_{\Omega_{\text{pix}}(\boldsymbol{\xi})} \cos \theta(\boldsymbol{\xi}), d\Omega \right] a^2 E(\theta(\boldsymbol{\xi}), \varphi(\boldsymbol{\xi})) d\xi d\eta. \quad (25)$$

Under the assumption of small variations of Ω_{pix} , θ , and E across the footprint (paraxial regime, planar scene, uniform distance), the term in square brackets and E can be treated as constants, and thus

Approximate scene-based form of the optogeometric factor

$$F_{\text{opg}}^{(\text{scene})} \approx \left(\iint_{\Omega_{\text{pix}}} \cos \theta \, d\Omega \right) \underbrace{\int_{-1/2}^{1/2} \int_{-1/2}^{1/2} a^2 E(\theta, \varphi) \, d\xi \, d\eta}_{A_{\text{fp}}} = A_{\text{fp}} \Omega_{\text{pix}}^{(\cos)}, \quad (26)$$

where $\Omega_{\text{pix}}^{(\cos)} = \iint_{\Omega_{\text{pix}}} \cos \theta, \, d\Omega$; [sr] is the cosine-weighted solid angle, and $A_{\text{fp}} = \int a^2 E, \, d\xi, \, d\eta$ [m²] is the effective footprint.

3.3 Geometrical (scene-based) derivation of the optogeometric factor

We begin with the scene-based pixel-level form for Φ_{pix} , valid for spatially and angularly uniform scene radiance,

$$\Phi_{\text{pix}} = L_{\text{scene}} \cdot F_{\text{opg}}^{(\text{scene})}. \quad (27)$$

Approximate form: Under idealized geometric and optical conditions (Table 1), the scene-based optogeometric factor can be approximated as

$$\tilde{F}_{\text{opg}}^{(\text{scene})} = A_{\text{fp}} \cdot \Omega_{\text{pix}}, \quad (28)$$

where the tilde notation explicitly denotes an approximate value. This expression corresponds to the *local étendue* [16, 17, 20] associated with the coupling between the pixel and its corresponding scene element.

Paraxial explicit form: In the paraxial (small-angle) approximation, the footprint area A_{fp} and the pixel's acceptance solid angle Ω_{pix} can be expressed as

$$A_{\text{fp}} \approx \left(\frac{a_{\text{pix}} d}{f} \right)^2, \quad \Omega_{\text{pix}} \approx \left(\frac{a_{\text{pix}}}{f} \right)^2, \quad (29)$$

where a_{pix} [m] is the pixel pitch, f [m] is the focal length, and d [m] is the object distance.

Substituting (29) into Eq. (28) yields two equivalent forms of the scene-based optogeometric factor:

$$\tilde{F}_{\text{opg}}^{(\text{scene})} \approx \frac{a_{\text{pix}}^4 d^2}{f^4} = A_{\text{fp}} \cdot \varphi_{\text{iFOV}}^2, \quad (30)$$

where $A_{\text{fp}} \approx (a_{\text{pix}} d/f)^2$ is the projected pixel footprint area on the object plane and $\varphi_{\text{iFOV}} \approx a_{\text{pix}}/f$ is the instantaneous field of view per pixel (in radians).

The first form in Eq. (30) highlights the direct dependence on pixel pitch, focal length, and object distance; the second form emphasises the product of the projected footprint area and the squared iFOV, mirroring the structure of the sensor-based formulation in Eq. (39).

Pupil-based scene formulation: Using $A_{\text{fp}} \approx (d \varphi_{\text{iFOV}})^2$ and the small-angle solid angle of a circular entrance pupil as seen from the scene point, $\Omega_{\text{pix}} \approx \frac{\pi}{4} \left(\frac{D}{d}\right)^2$, we obtain

$$\tilde{F}_{\text{opg}}^{(\text{scene})} \approx A_{\text{fp}} \Omega_{\text{pix}} = (d \varphi_{\text{iFOV}})^2 \frac{\pi}{4} \left(\frac{D}{d}\right)^2. \quad (31)$$

If the circular-aperture solid angle is defined in the small-angle form $\Omega_{\text{ap}} \approx \frac{\pi D^2}{4f^2}$, the paraxial scene-based expression can be written as

Compact form of the optogeometric factor

$$\tilde{F}_{\text{opg}}^{(\text{scene})} \approx \frac{\pi}{4} (D \varphi_{\text{iFOV}})^2 \quad (32)$$

where the factor π originates from the circular-aperture solid-angle definition and is therefore already included in this form.

Condition	Description
Planar scene	Observed surface is planar and oriented perpendicular to the optical axis.
Uniform distance	All points within the pixel footprint are at the same object distance d .
Paraxial approximation	Pixel pitch a_{pix} is small relative to focal length f , so that $\tan \theta \approx \theta$.
Pure projection geometry	Pixel footprint is determined solely by geometric projection, without distortion or vignetting.
Uniform radiance	Scene radiance is spatially uniform over the entire pixel footprint.

Table 1: Modelling assumptions under which the approximate form $\tilde{F}_{\text{opg}}^{(\text{scene})}$ in Eq. (28) equals the exact scene-based $F_{\text{opg}}^{(\text{scene})}$.

3.4 Optical (sensor-based) derivation

From the general radiometric relationship

$$\Phi_{\text{pix}} = L_{\text{sensor}} \cdot F_{\text{opg}}, \quad (33)$$

the *sensor-based* interpretation of F_{opg} is obtained by expressing it as the product of the physical collecting area of a single pixel in the detector plane, A_{pix} [m²], and the

cosine-weighted solid angle Ω_{ap} [sr] subtended by the camera aperture as seen from that pixel:

$$F_{\text{opg}}^{(\text{sensor})} := A_{\text{pix}} \Omega_{\text{ap}}. \quad (34)$$

This form directly relates the optogeometric factor to measurable sensor parameters, without requiring prior knowledge of the scene geometry.

The relevant collecting area is the physical pixel area

$$A_{\text{pix}} = a_{\text{pix}}^2, \quad (35)$$

where a_{pix} [m] is the pixel pitch. The solid angle of a circular aperture of diameter D [m] at focal length f [m], in the small-angle (paraxial) limit, is

$$\Omega_{\text{ap}} \approx \frac{\pi}{4} \left(\frac{D}{f} \right)^2. \quad (36)$$

Approximate form. Under the above assumptions, the sensor-based optogeometric factor can be written as

$$\tilde{F}_{\text{opg}}^{(\text{sensor})} = A_{\text{pix}} \cdot \Omega_{\text{ap}} \approx a_{\text{pix}}^2 \cdot \frac{\pi}{4} \left(\frac{D}{f} \right)^2. \quad (37)$$

Paraxial explicit form: Using the f-number definition

$$f\# = \frac{f}{D}, \quad (38)$$

and absorbing the factor π into the definition of the small-angle circular-aperture approximation for convenience, Eq. (37) becomes

Final compact form of the optogeometric factor

$$F_{\text{opg}} \approx \frac{\pi}{4} \left(\frac{f}{f\#} \right)^2 \left(\frac{a_{\text{pix}}}{f} \right)^2 = \frac{\pi}{4} \left(\frac{a_{\text{pix}}}{f\#} \right)^2. \quad (39)$$

This final form shows that, in the paraxial limit, the sensor-based optogeometric factor depends only on the pixel pitch and the f-number of the optics, and is independent of the object distance d . It mirrors the structure of the scene-based expression in Eq. (30), ensuring symmetry between the two derivations.

Condition	Description
Paraxial approximation	Pixel pitch a_{pix} is small relative to focal length f , so $\tan \theta \approx \theta$.
Circular aperture	Entrance pupil is circular, with diameter D .
No vignetting	Aperture is fully illuminated across the entire field of view.
Negligible diffraction	Optical resolution is limited by pixel size, not by diffraction.
Uniform transmittance	Optical transmittance is constant over the entire aperture.

Table 2: Modelling assumptions under which the approximate form $\tilde{F}_{\text{opg}}^{(\text{sensor})}$ in Eq. (39) equals the exact sensor-based $F_{\text{opg}}^{(\text{sensor})}$.

3.5 Summary, comparison and special case

Equating the approximate scene-based form (14) and the sensor-based form (15) gives

$$d^2 \left(\frac{a_{\text{pix}}}{f} \right)^4 \approx \frac{\pi}{4} \left(\frac{a_{\text{pix}} D}{f^2} \right)^2. \quad (40)$$

These expressions yield identical results when $d = f$, corresponding to the special case where the object is placed at the focal distance and the image is formed directly in the focal plane. While this condition is *not* required for the validity of either derivation, it serves as a convenient internal consistency check. In practical thermal imaging, the typical operating regime is $d \gg f$.

The two main expressions for the optogeometric factor can be summarised as follows:

1. Scene-based (approximate):

$$\tilde{F}_{\text{opg}}^{(\text{scene})} = A_{\text{fp}} \Omega_{\text{pix}} \approx d^2 \left(\frac{a_{\text{pix}}}{f} \right)^4.$$

2. Sensor-based (paraxial, circular aperture; approximate):

$$\tilde{F}_{\text{opg}}^{(\text{sensor})} = A_{\text{pix}} \Omega_{\text{ap}} \approx a_{\text{pix}}^2 \frac{\pi}{4} \left(\frac{D}{f} \right)^2 = \frac{\pi}{4} \left(\frac{a_{\text{pix}}}{f\#} \right)^2.$$

Both expressions describe the same physical quantity in their respective approximate forms and can be transformed into one another through the imaging geometry and lens parameters.

These formulations are equivalent in the approximate sense, i.e.

$$\tilde{F}_{\text{opg}}^{(\text{scene})} = \tilde{F}_{\text{opg}}^{(\text{sensor})}, \quad (41)$$

under the paraxial approximation $\varphi_{\text{iFOV}} \approx a_{\text{pix}}/f$, which directly links the instantaneous field of view to the pixel pitch and focal length.

Condition	Assumption description
Planar scene	The observed surface is planar and oriented perpendicular to the optical axis.
Known distance	The scene is located at a uniform distance d from the camera.
Paraxial approximation	Pixel pitch a_{pix} is small relative to the focal length f , so that $\tan \theta \approx \theta$.
Pure projection geometry	Pixel footprint is determined solely by geometric projection, with no lens distortion or vignetting.
Uniform radiance	Radiance is spatially uniform over the pixel footprint.
Circular aperture	Entrance pupil is circular; in the paraxial approximation, $\Omega_{\text{ap}} \approx \frac{\pi}{4} \left(\frac{D}{f}\right)^2$.
No diffraction effects	Aperture D is sufficiently large relative to wavelength λ so that diffraction does not significantly affect Ω_{ap} .
Constant transmittance	Optical transmittance is constant over the field of view.

Table 3: Modelling assumptions under which $\tilde{F}_{\text{opg}}^{(\text{scene})} \approx \tilde{F}_{\text{opg}}^{(\text{sensor})}$ holds.

3.6 Example determination of the optogeometric factor for real thermal imaging systems

This section verifies the *numerical equivalence* of the two theoretically derived expressions for the optogeometric factor, Eqs. (39) and (32), using representative specifications of real thermal imaging systems. The aim is to demonstrate that both formulations — (i) based on the pixel pitch-to-f-number ratio and (ii) based on the product of the entrance pupil diameter and the instantaneous field of view — yield identical values of F_{opg} when applied under the same optical and geometric assumptions.

The example parameters listed in Tables 4 and 5 are *not experimental measurements*, but are taken directly from published datasheets and literature sources [3, 12, 13]. They represent typical LWIR and MWIR detector–optics configurations, chosen solely to illustrate the calculation procedure.

System	a_{pix} [m]	$f\#$	$a_{\text{pix}}/f\#$ [m]	F_{opg} [m ² sr]
LWIR 17 μm f/1.0	1.70×10^{-5}	1.0	1.70×10^{-5}	2.27×10^{-10}
LWIR 25 μm f/1.1	2.50×10^{-5}	1.1	2.27×10^{-5}	4.06×10^{-10}
MWIR 15 μm f/2.0	1.50×10^{-5}	2.0	7.50×10^{-6}	4.42×10^{-11}
MWIR 15 μm f/2.5	1.50×10^{-5}	2.5	6.00×10^{-6}	2.83×10^{-11}

Table 4: Optogeometric factor F_{opg} calculated via $F_{\text{opg}} = \frac{\pi}{4} \cdot (a_{\text{pix}}/f\#)^2$ using the pixel pitch / f-number ratio. System parameters are taken from [3, 12, 13].

System	f [m]	$f\#$	D [m]	φ_{iFOV} [rad]	F_{opg} [m ² sr]
LWIR 17 μm f/1.0	1.30×10^{-2}	1.0	1.30×10^{-2}	1.31×10^{-3}	2.28×10^{-10}
LWIR 25 μm f/1.1	9.00×10^{-3}	1.1	8.18×10^{-3}	2.78×10^{-3}	4.06×10^{-10}
MWIR 15 μm f/2.0	2.50×10^{-2}	2.0	1.25×10^{-2}	6.00×10^{-4}	4.42×10^{-11}
MWIR 15 μm f/2.5	1.00×10^{-1}	2.5	4.00×10^{-2}	1.50×10^{-4}	2.83×10^{-11}

Table 5: Optogeometric factor F_{opg} calculated via $F_{\text{opg}} = \frac{\pi}{4} \cdot (D \cdot \varphi_{\text{iFOV}})^2$. System parameters are taken from [3, 12, 13].

The tabulated values confirm that both calculation routes yield identical results to within numerical precision, providing a strong validation of the theoretical derivation. This consistency holds provided that the underlying assumptions (paraxial approximation, uniform radiance, ideal projection geometry, and known $f\#$) are satisfied.

3.7 Effective optogeometric factor

In practical detector designs, the entire geometrical pixel area defined by the pitch a_{pix} is not fully photosensitive or thermosensitive. Non-sensitive borders and inter-pixel gaps, often required for isolation or readout circuitry, do not contribute to the conversion of incident radiant power into electrical signal. The fraction of the area of the pixels that is photosensitive is characterized by the *fill factor* FF [–] [4], defined as

$$\text{FF} := \frac{A_{\text{active}}}{A_{\text{pixel}}}, \quad (42)$$

where A_{active} is the photosensitive area and A_{pixel} is the total geometrical pixel area corresponding to the pitch a . The concept is illustrated in Fig. 3.

Since the optogeometric factor F_{opg} in equation (39) is derived from the geometrical pixel footprint, it represents the maximum possible optical coupling, i.e., the radiant power that would be collected if the entire area of the pixels is sensitive. In reality, only the active area of the pixel, corresponding to a fraction FF of its total area, captures the incident radiation and converts it into signal. This leads to the definition of the *effective optogeometric factor*:

$$F_{\text{opg,eff}} := F_{\text{opg}} \cdot \text{FF}. \quad (43)$$

This correction is particularly relevant for sensors with small pixel pitches, where inter-pixel gaps and non-sensitive structures occupy a significant fraction of the pixel footprint. In such cases, neglecting the fill factor may lead to an overestimation of the radiant power incident on the active area, and consequently to an underestimation of measurement uncertainty.

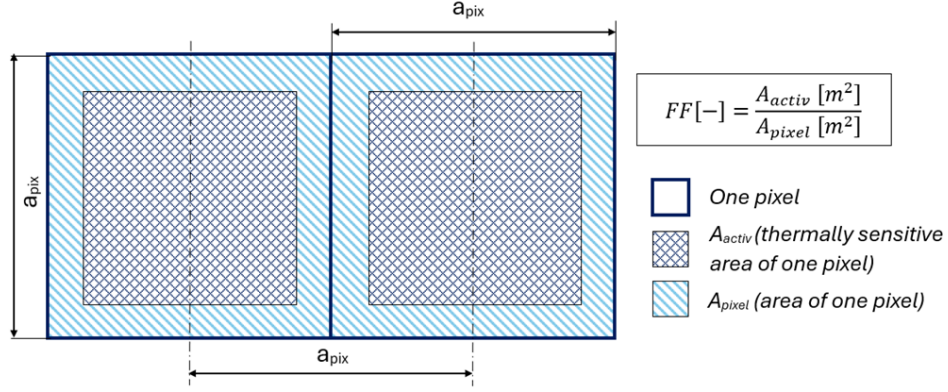


Figure 3: The figure illustrates two pixels of a thermal camera with a pixel pitch a_{pix} [m], showing the distinction between the active area A_{activ} [m²] and the total pixel area A_{pixel} [m²]. The total pixel area A_{pixel} corresponds to the full geometrical extent of one pixel, including regions that are not sensitive to incident thermal radiation. The active area A_{activ} corresponds to the portion of the pixel that is sensitive to incident thermal radiation. The fill factor FF [-] is then defined as $FF = \frac{A_{\text{activ}}}{A_{\text{pixel}}}$.

4 Discussion

4.1 Occurrence of the Optogeometric Factor in Literature

To the best of the authors' knowledge, the optogeometric factor F_{opg} , as defined in this work, has not previously been reported in such an explicit, pixel-level form in the thermographic literature, with the sole exception of [1], where it appeared implicitly as part of the derivation of the quantitative thermography equation. Here, we formalise F_{opg} as a concise and physically transparent quantity that directly links pixel-level geometry to the radiant power delivered through the optical path.

Upon review, closely related expressions are found in several distinct domains of optics and radiometry—often under different names, in different contexts, and without explicit identification as a standalone factor:

- **Classical radiometry:** The fundamental relation

$$\Phi = L \cdot A \cdot \Omega$$

appears in authoritative sources [15–17], typically applied at the system level. Geometrical derivations yield expressions such as

$$\Omega = \frac{A_{\text{aperture}}}{f^2} = \frac{\pi}{4(f\#)^2}, \quad A \cdot \Omega = A \cdot \frac{\pi}{4(f\#)^2},$$

which describe optical throughput in terms of aperture size and f-number [15, 17, 21]. However, these are not localised to pixel geometry, nor do they incorporate the pixel pitch a or connect explicitly to the thermography or quantitative imaging equation.

- **Technical implementations:** Optical design software such as Zemax OpticStudio [18] and TracePro [19] employs dependencies of the form $(a/f\#)^2$ or $(D \cdot a/f)^2$ in ray-tracing and irradiance calculations. Similarly, CMOS sensor modelling often includes comparable terms when analysing microlens efficiency and fill-factor effects. In both cases, the expressions embody the same geometric-optical coupling as F_{opg} , but remain embedded within optimisation routines without being formalised as independent radiometric parameters.

In summary, the expression (39) is grounded in established physical principles and directly related to radiometric throughput and étendue, yet it has not previously been presented, named, and systematically analysed in the context of infrared thermography. This work is, to the authors' knowledge, the first to provide such a definition and framework.

4.2 Paradigm Shift in Quantitative Thermography and Radiometry

The modelling framework introduced in [1] and extended here replaces the traditional, instrument-specific calibration paradigm with a physics-based, modular formulation. In conventional practice, the link between the measured signal and scene temperature is often described by empirical calibration curves, in which optical, geometric, and atmospheric effects are embedded within composite parameters. While such models can be tuned for a specific instrument, they lack physical transparency and are not readily transferable across configurations.

The present approach isolates these effects through the explicit definition of the *opto-geometric factor* F_{opg} and its fill-factor-adjusted counterpart $F_{\text{opg,eff}}$. This separation assigns:

- pixel geometry to F_{opg} ,
- detector design to the fill factor,
- optical and atmospheric effects to independent multiplicative terms.

Each term is measurable, verifiable, and directly propagates into the uncertainty budget.

This modular structure simplifies the physics rather than complicating it: radiometric coupling is expressed through quantities with clear physical meaning, enabling straightforward interpretation and standardised calibration procedures. The result is a unified, metrologically rigorous basis for quantitative thermography that bridges theoretical modelling and practical implementation.

In effect, the methodology shifts the focus from empirical, instrument-bound calibration toward a general, system-level model grounded in radiometric first principles. This not only improves accuracy and traceability, but also ensures adaptability and comparability of thermographic measurements across different systems and application domains.

A key distinction from conventional radiometric parameters (e.g., classical étendue) is that F_{opg} is *localised at the pixel level* and can be directly integrated into measurement equations, such as the quantitative thermography equation, without additional geometric factors. This represents a genuinely new formulation—making the introduction of a named quantity fully justified.

4.3 Limitations and Conditions of Validity

The analytical expression for the optogeometric factor (39) is derived under a set of modelling assumptions that restrict its applicability to specific measurement conditions and optical configurations. These assumptions — together with the corresponding equations for which they apply — are summarised in Tables 1, 2, and 3. The main conditions and limitations are as follows:

(i) Diffuse (Lambertian) emission: The derivation assumes isotropic surface radiance, i.e., Lambertian emission [8, 11]. For specular, glossy, or anisotropic surfaces, the directional dependence of emissivity becomes significant, and the assumption $L(\theta, \phi) = \text{const}$ no longer holds. In such cases, F_{opg} can no longer be treated as a simple geometric scaling factor, and a more complex angular radiance model is required. Relevant conditions: *uniform radiance* in Table 1 and Table 3.

(ii) Paraxial geometry and small angles: The derivation employs the paraxial approximation, valid for small angular deviations from the optical axis (typically up to 50° – 60°). At larger viewing angles, second-order geometric effects and vignetting may reduce the effective radiance collection, and the assumption of angle-independent radiant flux breaks down. Relevant equations: (4), (39). Relevant conditions: *paraxial approximation* in Tables 1, 2, and 3.

(iii) Planar target surfaces: The model presumes locally planar measured surfaces. For curved or structured surfaces, especially with high curvature within a single pixel’s iFOV, the pixel footprint is no longer a simple projection, and radiometric integration over the solid angle becomes nontrivial. Relevant conditions: *planar scene* in Tables 1 and 3.

(iv) Fixed optical configuration: The optogeometric factor is sensitive to variations in optical geometry. In particular, changes in the effective focal length f (e.g., due to focusing mechanisms) affect the f-number and thereby F_{opg} according to equation (39).

(v) Ideal sensor pixel geometry: The derivation assumes square pixels with well-defined pitch a_{pix} as in equation (6). For sensors with asymmetric pixel layouts or significant fill-factor variation across the array, the geometric projection and radiometric

response may deviate from the ideal model, necessitating empirical correction. Relevant conditions: *pixel pitch* a_{pix} *well-defined* in Table 2.

(vi) Absence of optical vignetting and internal emission: The model neglects internal emission from optical elements and assumes no significant vignetting. These effects are generally minor in well-designed thermal systems but may become relevant in high-precision or low-signal applications. Relevant conditions: *no vignetting* in Table 2 and *no diffraction effects* in Table 3.

Taken together, these limitations do not challenge the fundamental validity of the derived expression under standard thermographic conditions. Rather, they define the conditions under which the applicability of the optogeometric factor should be carefully evaluated.

4.4 Analogy to Electrical Resistance

The analogy is straightforward:

- **Electrical resistance** R relates voltage and current:

$$U = I \cdot R$$

where R encapsulates the properties of the conductor (material, length, cross-sectional area) into a single quantity.

- **Optogeometric factor (sensor-based)** $F_{\text{opg}}^{(\text{sensor})}$ relates the radiance at the sensor's focal plane to the captured radiant flux:

$$\Phi_{\text{pix}} = L_{\text{sensor}} \cdot F_{\text{opg}}^{(\text{sensor})}$$

where L_{sensor} [$\text{W m}^{-2} \text{sr}^{-1}$] is the radiance at the sensor focal plane after all optical effects, and $F_{\text{opg}}^{(\text{sensor})}$ [$\text{m}^2 \text{sr}$] encapsulates the properties of the sensor pixel geometry and its associated optics into a single quantity.

Just as the electrical resistance allows any conductor to be described by a single number, $F_{\text{opg}}^{(\text{sensor})}$ allows any pixel–optics configuration to be described by a single numerical characteristic of *radiometric throughput*, with units of $\text{m}^2 \text{sr}$.

4.5 Illustrative example (approximate): uniform blackbody scene

Consider an ideal blackbody of uniform temperature T , neglecting atmospheric effects and assuming uniform radiance over the pixel footprint. The Stefan–Boltzmann law gives the hemispherical exitance

$$M = \sigma T^4$$

and the corresponding radiance

$$L_{\text{bb}}(T) = \frac{\sigma T^4}{\pi}, \quad (44)$$

where σ [$\text{W m}^{-2} \text{K}^{-4}$] is the Stefan–Boltzmann constant. The factor $1/\pi$ comes from the Lambertian relationship between hemispherical exitance M and radiance L .

In the paraxial limit, and for a scene radiance $L_{\text{scene}} = L_{\text{bb}}(T)$, the pixel-integrated radiant flux is

Approximate pixel flux for a uniform blackbody scene

$$\Phi_{\text{pix}} \approx \frac{\sigma T^4}{\pi} \cdot \frac{\pi}{4} \left(\frac{a_{\text{pix}}}{f\#} \right)^2 = \frac{\sigma T^4}{\pi} \cdot \tilde{F}_{\text{opg}}^{(\text{scene})} \quad (45)$$

where $\tilde{F}_{\text{opg}}^{(\text{scene})}$ is the scene-based approximation of the optogeometric factor, defined purely from pixel geometry and optics, *without* the π factor.

This expression makes it explicit that the π originates from the blackbody radiance relation and is not part of the optogeometric factor itself. Under these idealised assumptions, Φ_{pix} is simply proportional to T^4 and to the square of the pixel pitch-to- $f\#$ ratio.

5 Conclusion

The *optogeometric factor* F_{opg} has been introduced as a physically transparent, pixel-level descriptor of geometric-optical throughput with units of $\text{m}^2 \text{sr}$. Two alternative formulations have been derived: a scene-based form, relying on the projected footprint and acceptance solid angle, and a sensor-based form, relying on pixel pitch and optical f -number. It has been demonstrated analytically, and illustrated numerically for representative thermal imaging configurations, that these formulations produce identical results under paraxial, ideal-projection conditions with uniform scene radiance.

By isolating F_{opg} from other radiometric terms, a unified and transferable parameter is provided that can be directly integrated into quantitative imaging equations. The effective form, $F_{\text{opg,eff}}$, extends the concept to real detectors with finite fill factor, enabling more accurate modelling of practical systems.

Beyond quantitative thermography, the optogeometric factor is applicable to other imaging modalities operating in the geometric-optics regime, providing a standardised parameter for describing and comparing pixel-level radiometric coupling.

References

- [1] M. Hofreiter and J. Sova and M. Kolaříková and L. Kolařík and T. Němec, *Thermography Equation for Non-Perpendicular Infrared Measurements: Derivation, Analy-*

- sis, and Experimental Validation*, Infrared Physics and Technology, 2025, p. 106010, doi:10.1016/j.infrared.2025.106010.
- [2] L. Forejtová and T. Zavadil and L. Kolařík and M. Kolaříková and J. Sova and P. Vávra, *Non-destructive inspection by infrared thermography of resistance spot welds used in automotive industry*, Acta Polytechnica, 2019, p. 238–247, doi:10.14311/AP.2019.59.0238.
- [3] A. Daniels, *Field Guide to Infrared Systems, Detectors, and FPAs, Third Edition*, 2018, doi:10.1117/3.2315935.
- [4] G. C. Holst, *Electro-Optical Imaging System Performance*, 2017, doi:10.1117/3.2588947.
- [5] Rogalski, A. and Chrzanowski, K., *Infrared Devices And Techniques (Revision)*, Metrology and Measurement Systems, 2014 p. 565–618, doi:10.2478/mms-2014-0057.
- [6] Chartier, Germain, *Introduction to Optics*, 2005, p. XVIII, 598, doi:10.1007/b106780.
- [7] Cukor, Jan and Bartoška, Jan and Rohla, Jan and Sova, Jan and Machálek, Antonín, *Use of aerial thermography to reduce mortality of roe deer fawns before harvest*, PeerJ, 2019, p. e6923, doi:10.7717/peerj.6923.
- [8] M. Vollmer and K. P. Möllmann, *Infrared Thermal Imaging: Fundamentals, Research and Applications*, 2010,
- [9] Waldemar Minkina and Sebastian Dudzik, *Infrared Thermography: Errors and Uncertainties*, 2009, doi:10.1002/9780470682234.
- [10] Eugene Hecht, *Optics*, 2016.
- [11] F. E. Nicodemus, *Reflectance Nomenclature and Directional Reflectance and Emissivity*, Appl. Opt., 1970, p. 1474–1475, doi:10.1364/AO.9.001474.
- [12] R.K. Bhan and V. Dhar, *Recent infrared detector technologies, applications, trends and development of HgCdTe based cooled infrared focal plane arrays and their characterization*, Opto-Electronics Review, 2019, p. 174–193, doi:https://doi.org/10.1016/j.opelre.2019.04.004.
- [13] P.V. Karthik Yadav and Isha Yadav and B. Ajitha and Abraham Rajasekar and Sudha Gupta and Y. Ashok Kumar Reddy, *Advancements of uncooled infrared microbolometer materials: A review*, Sensors and Actuators A: Physical, 2022, p. 113611, doi:https://doi.org/10.1016/j.sna.2022.113611.
- [14] International Organization for Standardization, *ISO 9334 - Optics and photonics — Optical transfer function — Definitions and mathematical relationships*, 2012,
- [15] Grant, Barbara G., *Field Guide to Radiometry*, 2011.
- [16] William R. McCluney, *Introduction to Radiometry and Photometry*, 1994.
- [17] Robert W. Boyd, *Radiometry and the Detection of Optical Radiation*, 1983.
- [18] Radiant ZEMAX LLC, *ZEMAX Optical Design Program User's Manual*, 2011.

- [19] Lambda Research Corporation, *TracePro User Guide*, 2025.
- [20] Goodman, Joseph W., *Introduction to Fourier Optics*, 1996,
- [21] Howell, John R. and Mengüç, M. Pinar and Daun, Kyle and Siegel, Robert, *Thermal Radiation Heat Transfer*, 2020, doi:10.1201/9780429327308.